Aerodynamic design, characterization and flight performance of RLV-TD

G. Vidya*, K. Manokaran, V. R. Ganesan, M. Prasath, Sundeepkumar Epuri, P. Balasubramanian, C. Babu, B. Venkatasubrahmanyam and Priyankar Bandyopadhyay

Aeronautics Entity, Vikram Sarabhai Space Centre, Indian Space Research Organisation, Thiruvananthapuram 695 022, India

Complete aerodynamic design and characterization of ascent as well as descent phases of Reusable Launch Vehicle-Technology Demonstrator (RLV-TD) have been obtained through thousands of wind tunnel tests, flow simulations using various computational fluid dynamic codes and tailor-made engineering codes. The evolution of the ascent and descent designs, aerodynamic characterization and flight performance is presented in this article. The flight data comparison of aerodynamic coefficients, control surface loads, pressure distribution and external acoustic levels with preflight data is good and therefore, providing confidence in using the ground-based data generation techniques along with defined dispersion bands. Some of the minor deviations in the performance observed in flight were resolved/understood in the post-flight analysis, whereas few effects observed in flight need further understanding.

Keywords: Aerodynamic design and characterization, ascent and descent phases, flight performance, Reusable Launch Vehicle, wing body.

Introduction

AERODYNAMICS plays a vital role in deciding the overall capability of a flying machine and aerodynamic inputs are used for the design and analyses of various systems such as structure, trajectory, flight control system and simulation studies. The data are generated using wind tunnel testing, computational fluid dynamics (CFD) simulations and empirical/engineering methods. The uncertainties on the aerodynamic coefficients are different from that of the conventional launch vehicle and more complex due to a large number of variables.

In this article, a brief description of the wing body Reusable Launch Vehicle-Technology Demonstrator (RLV-TD) configuration design and its evolution, aerodynamic characterization and flight performance are presented.

*For correspondence. (e-mail: g_vidya@vssc.gov.in)

RLV-TD configuration design evolution (descent phase)

The objective of this RLV-TD hypersonic experiment (HEX) mission is to demonstrate the technologies related to a future reusable two-stage-to-orbit (TSTO) vehicle of Indian Space Research Organisation (ISRO). The challenges involved in the configuration design are outlined in Box 1. (1) Desirable lift-to-drag ratio at hypersonic Mach numbers and high angles of attack during re-entry, in order to limit the deceleration levels to reasonable value and, achieve the required down range and cross range. (2) Provide adequate longitudinal, directional and lateral controllability using elevon and rudder in the high dynamic pressure regime and using Reaction Control System (RCS) jets also in low dynamic pressure regime. (3) Provide sufficient lift-to-drag ratio at low speeds to limit the sink rate. (4) Minimize the aerodynamic heating to an acceptable level for the given material. (5) Minimize the centre of pressure movement with Mach number. (6) Sizing of the fins in the ascent configuration to ensure controllability in all the axes and to reduce the static instability. (7) Flat-bottom surface of the fuselage for ease of placement of tiles. (8) Sufficient fuselage volume to accommodate avionics packages, actuators, batteries, RCS fuel tanks and thrusters, etc.

Design choices

In order to meet the given mission requirements, the lifting body and wing-body configurations are considered.

Box 1. Design requirements in descent vehicle.

- Adequate aerodynamic efficiency (L/D; subsonic ~5 and hypersonic ~2).
- RCS jets used for 3 axes control at low dynamic pressure conditions.
- Stability and controllability at all flight regimes. Control surface deflections limited to ±30°.
- Lift to support overall mass of the TDV (~1750 kg).
- Touchdown velocity, V_{TD} < 80 m/s @ angle of attack 15°.
- Maximum load factor <4 g.
- q-heat flux in the stagnation region <60 W/cm^2.

Lifting bodies have low lift-to-drag (L/D) ratio and hence low cross and downrange and gliding capability. On the other hand, the wing body configuration has high L/D in subsonic as well as hypersonic speeds, which gives better cross and downrange. The wing-body configuration is selected to provide high aerodynamic efficiency. To arrive at the geometrical details of this configuration, database of winged-body vehicles having similar mission profile is used for arriving at nominal values and trade-off studies are carried out to assess the effect of various parameters on the vehicle aerodynamic characteristics. Final values of vehicle parameters are selected to meet the mission requirements.

Fuselage with ogive-shaped forebody, low-aspect-ratio double-delta wing with single vertical tail was the first configuration for which extensive wind tunnel testing was carried out. Figure 1 shows the RLV-TD configuration with single vertical tail wing-body configuration with body flap.

Figure 2 shows the experimental and PARAS-3D CFD[1] results for pitching moment coefficient (cm) as a function of angle of attack (α) at Mach number (M) = 2, along with engineering estimate using 'WTAP'[2]. Even an upward elevon deflection of –20° results in trim at 0° angle of attack only at Mach number 2.0. Therefore, changes in the configuration were necessary to improve longitudinal controllability, especially at supersonic conditions.

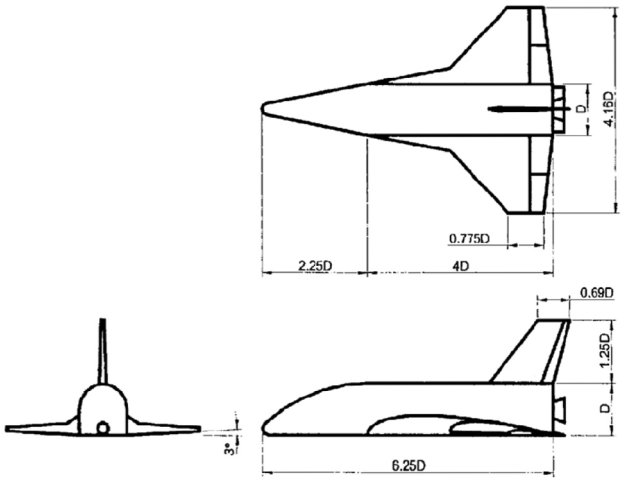

Figure 1. Reusable Launch Vehicle-Technology Demonstrator (RLV-TD) wing-body configuration with single vertical tail and body flap – one of the earlier configurations for which detailed characterization was carried out.

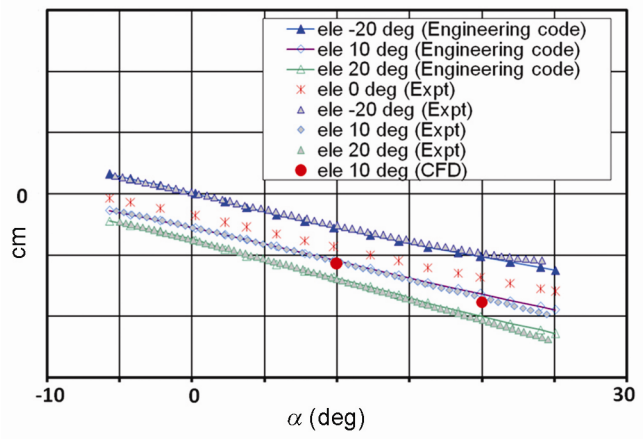

Figure 2. Single vertical tail configuration pitching moment characteristics with elevon deflections indicating trim issue at M = 2.0.

The wing airfoil was derived from NACA0012 with flat bottom surface. Further, the airfoil was reshaped from cambered to reflex type in order to reduce the excessive pitching moment. The reflex airfoil is S-shaped with negative camber for the aft 20% of the chord length to reduce the pitch down moment and bring it close to zero about the aerodynamic centre. The airfoil thickness-to-chord ratio was varied from 10% to 12% from root to tip of the wing span. The wing planform area was reduced without sacrificing lift requirements. The forebody was redesigned for better longitudinal controllability and to reduce the directional instability level at supersonic and hypersonic regimes. Body flap was removed due to the constraints during RLV-TD/HS9 booster separation. The single vertical tail was replaced with twin canted vertical tail because of better aerodynamic control. The twin canted vertical tail airfoil is a double-wedge type with maximum thickness at 60% of chord. The rudders are used for directional control and also as speed brakes and thus augment the vehicle trimmability in pitch (rudderva-tor). The fuselage configuration has to meet the volume requirement apart from the aerodynamic requirements. The fuselage has a blunt ogive forebody followed by D-section fuselage. The 'D' section with semicircle top and box-type bottom section is selected to facilitate (i) ease of thermal protection system (TPS) tile manufacturing and mounting on the bottom surface, and (ii) to have blended low wing configuration to reduce aerodynamic heating. The wing has a double-delta planform with 80° leading edge strake angle and 45° main wing leading edge angle. The 80°/45° wing planform delays the wing stall and reduces the centre of pressure movement over the operating range of Mach numbers. The wing has an aspect ratio of 2.16, 3° dihedral angle (wing tip section is at a higher level than the wing root section) and wing span of 0.55 times the vehicle length. RCS thrusters of 12 numbers were used for three axes controls during low dynamic pressure conditions. The pitch RCS thrusters were placed in the aft fuselage top and bottom surfaces, the yaw RCS thrusters were placed at the aft fuselage side panels and roll RCS thrusters were placed in the top and bottom surfaces of the wing. The control surface deflection was limited to ±30°. Figure 3 shows the finalized descent phase configuration.

RLV-TD configuration design evolution (ascent phase)

The ascent configuration is a tandem arrangement with a wing-body configuration on the top of a 9 tonne solid

rocket booster. The design is evolved by meeting various design criteria dictated by aerodynamics, aero elasticity, structures, propulsion and controls. The tandem arrangements resulted in a large aerodynamic instability about the centre of gravity. This instability is reduced by four fins placed on the base shroud near the base of the vehicle. The fins have both fixed and movable (outer) parts; the aerodynamic control is through the movable fins. During initial liftoff, where the dynamic pressure is very low, the pitch–yaw controls are achieved through secondary injection thrust vector controls (SITVC) and the roll control is through roll RCS thrusters. As the dynamic pressure builds up above 2 kPa, the movable fins are activated to control the vehicle in all three axes.

The major hurdle in the finalization of the ascent vehicle configuration is the high aerodynamic moment coefficient, i.e. μ_α (the ratio of aerodynamic moment about the centre of gravity to the moment of inertia about the pitch axis, also M_α/I_{yy}) of 20 (off-nominal 25) for the nominal case at Mach number 1.1, whereas in our expendable launch vehicles, μ_α ranges from 0.75 to 4.5. This parameter is a direct indication of how quickly a disturbance builds up in the form of angular acceleration. Even though the static control force which is available through the deflection of movable fins is more than the aerodynamic disturbance force, high μ_α posed difficulty in the autopilot design due to the aerodynamic control action not being fast enough to overcome the disturbance build-up.

The core base shroud length is (1.22 m long with 6° flare angle) fixed and hence, the root chord of the fin cannot be more than the core base shroud length unless over-hanging fin is desired. For the fin control, both all movable and movable tip fin options were studied and the latter was chosen. Therefore, the base of the fin has the fixed portion and the tip has the movable portion. The various fin planforms with span ranging from 1.2 to 2.0 m were studied to improve the high μ_α both in the nominal and off-nominal cases with acceptable aerodynamics (henceforth abbreviated to aero) and gain margins. The aero and gain margins for the launch vehicles are generally kept at 6 and 3 dB for nominal and off-nominal vehicle aero data respectively. However, this type of new configuration with wing body on the top may call for higher margins. Another aspect is that even if the vehicle is controllable with high μ_α due to large static control force, flexibility may result in a reduction in the gain margin. Therefore, the RLV-TD ascent vehicle configuration fin design has to meet the conflicting requirements of acceptable aero and gain margin for the required performance.

The outcome of various fin design studies indicated that the increase in root chord and leading edge sweep angle has little effect on μ_α, whereas, the increase in span improves μ_α. Thickness distribution and wedge angle are influenced by structural design and actuator mounting requirements, though the drag coefficient is affected adversely by these requirements. However, the off-nominal μ_α of 25 is feasible only when the aero margin is reduced to 1 dB with improved actuator bandwidth of 6.5 Hz. The final fin design was selected based on the control and structural dynamics consideration, where acceptable μ_α and normal force coefficient slope due to movable fin deflection, $C_{N\delta}$ (control surface effectiveness) were achieved. The ascent configuration shown has height which is 2.6 times the length of RLV-TD. There are four fins placed in X-configuration at the core base shroud to improve the longitudinal stability and controllability during ascent phase. Each fin has a fixed part and movable part for pitch, yaw and roll controls, with a limit of ±30 deg.

The effect of wake of the forebody on the fins is captured in the design cycle using CFD simulations and

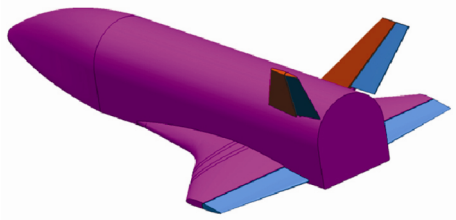

Figure 3. Finalized RLV-TD descent configuration with reflex wing and canted twin vertical tail with body flap removed.

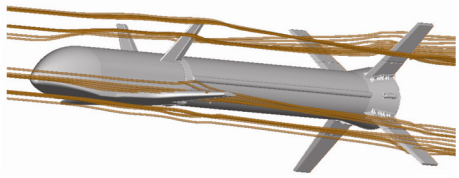

Figure 4. Volume lines from CFD simulation indicating interference flow field from wings and vertical tails over the aft fins.

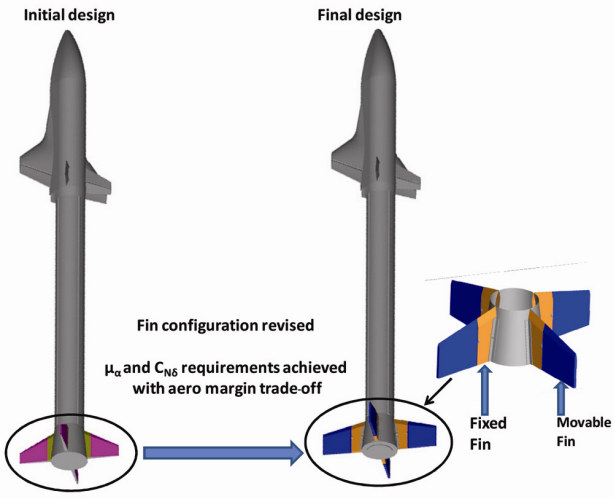

Figure 5. Evolution of RLV-TD ascent configuration with major changes in the fin design.

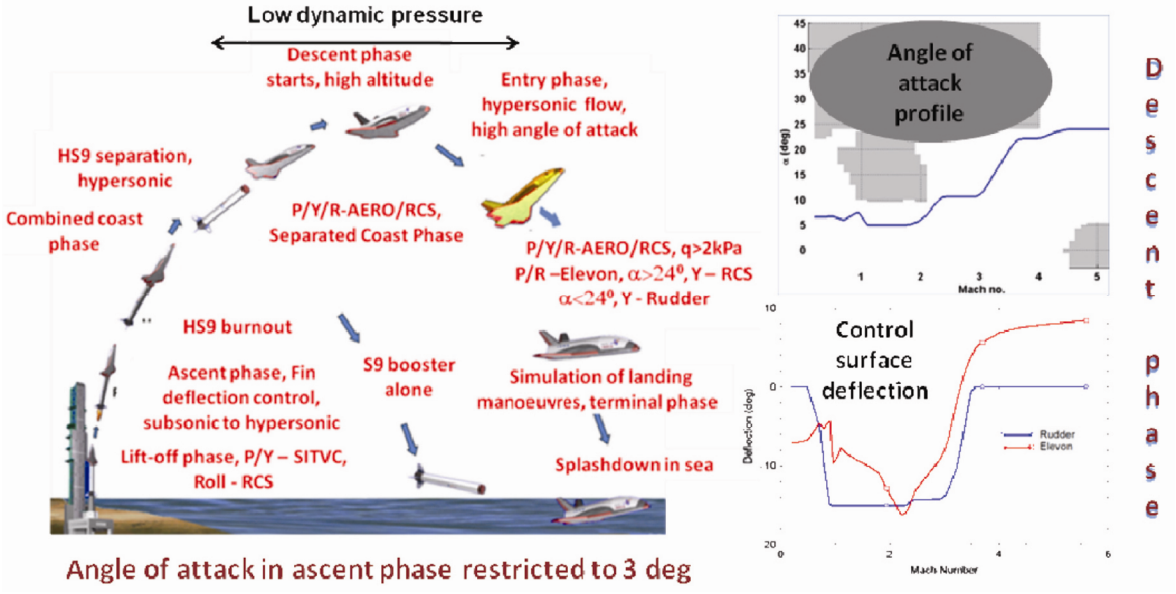

Figure 6. Overall mission sequence of RLV-TD from liftoff to splashdown in sea along with angle of attack and control surface deflection profile in the descent phase.

wind tunnel tests. The wake of the forebody, especially from the vertical tail (VT) and wing, passes over the fins placed at the aft (Figure 4), resulting in decrease of local angle of attack up to ~3 deg.

Figure 5 shows the ascent configuration design evolution, where the fin design is changed from 1.2 m span with 30 deg sweep to the final design of 1.5 m span with 15 deg sweep. Trailing edge sweep angle is 0 degree. The fin area was increased by ~70%, whereas the movable fin area was increased by ~45% to meet stability and control requirements (off-nominal μ_α of ~32 and $C_{N\delta}$ of ~0.6 at $M = 1.1$).

HEX mission profile

The overall mission sequence of RLV-TD is shown in Figure 6; and has the following salient features. The RLV-TD placed in tandem with HS9 booster, was lifted-off from SDSC-SHAR first launch pad. During lift-off, the vehicle experienced high angle of attack aerodynamics at low speeds. Roll RCS thrusters were used during the low dynamic pressure regime prevailing during liftoff for roll control. The vehicle attained low angle of attack after clearing the launch pad and was controlled by movable fin from subsonic to hypersonic Mach numbers. RLV-TD was separated from HS9 booster at high altitude, where the flow is hypersonic. The vehicle was re-oriented to high angle of attack using a combination of elevon deflection and yaw RCS firing. Upon entry into sensible atmosphere, the angle of attack was brought down to reasonable levels as the vehicle decelerated to lower altitudes and low supersonic Mach numbers. Below $M = 2$, closed loop guidance was used, where the angle of attack is small and the control is completely through elevon and rudder. The vehicle landed on virtual runway in the sea with allowable sink rate so that the structure was intact. Also, the trajectory was essentially planar, i.e. angle of sideslip was not commanded, but produced as a result of various disturbances only and was close to zero.

Based on the mission sequence, aerodynamic characterization can be broadly classified into: (1) low speed, liftoff regime with high angles of attack and launch pad proximity effects; (2) ascent flight with small angles of attack and fin deflection; (3) stage separation at hypersonic Mach number at small angles of attack; (4) high altitude phase where RCS thrusters and control surfaces are operated in combination at moderate to high angles of attack, and (5) Descent phase at supersonic to subsonic Mach numbers with varying angles of attack and control surface deflections. The aerodynamic characterization was carried out for various configurations according to various phases of flight.

The ascent phase mission profile is similar to launch vehicle mission profile, where angle of attack is small, but the difference lies in the aerodynamic characterization with fin deflections (elevons and rudders are always in null position), which increases the number of models and tests to an order of magnitude higher than that of a typical launch vehicle. During the descent phase, however, the complexity and database requirements are higher, since the number of variables increases (Mach number, angle of attack, angle of sideslip, elevon deflection, rudder deflection) and the range of angle of attack is also wider according to the entry phase mission requirements.

All the above factors drive the aerodynamic data requirements to a higher level than that involved in a typical launch vehicle. Database for a conventional

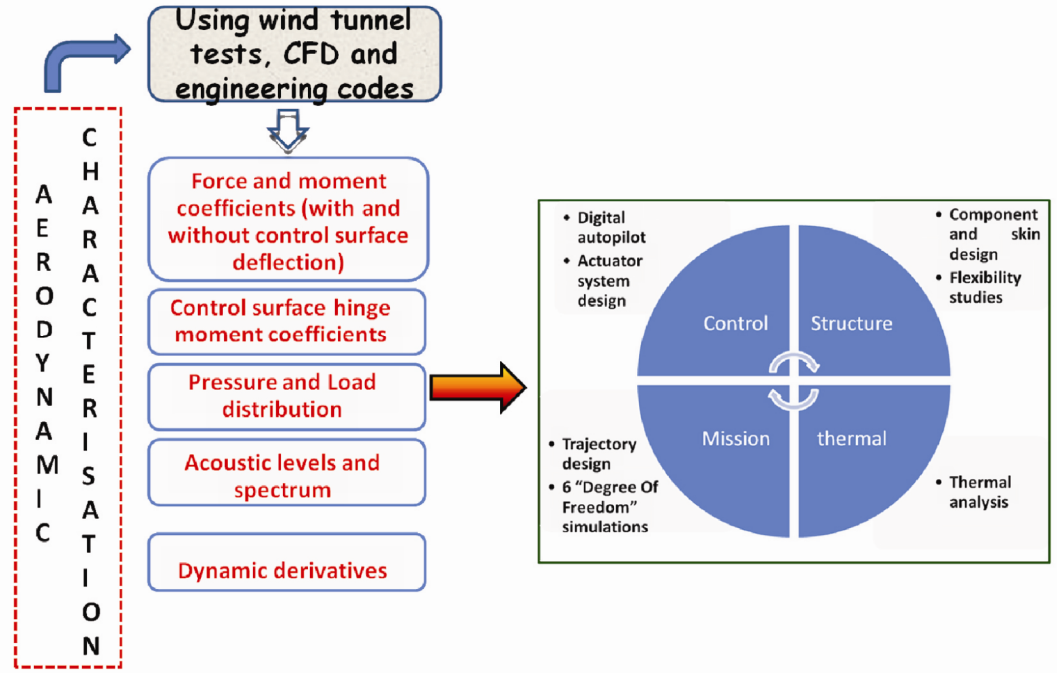

Figure 7. Aerodynamic characterization for generation of inputs to various disciplines.

expendable launch vehicle results in tens of data tables, whereas the database for RLV-TD is in thousands.

Aerodynamic characterization

CFD codes, and engineering methods based on a database were used for conceptual design and sizing of various components. PARAS-3D, a Cartesian grid-based CFD code was used extensively for configuration design trade-off studies. The message passing interface (MPI) based parallelization, capability to import CAD-based geometries, fully automatic grid generation and adaptation capability make it ideal for production simulations. Other CFD codes such as UNS3D, SU^2 (open source) and CFD++ (commercial code) were also used for design and analysis. SAGA (Supercomputer for Aerospace with GPU architecture) with a theoretical peak speed of 450 TeraFLOPS was exclusively used for thousands of CFD simulations in the design evolution phase and aerodynamic characterization phase.

Various wind-tunnel facilities such as 1 m hypersonic tunnel and 0.25 m hypersonic tunnel at VSSC, Thiruvananthapuram, trisonic wind tunnel at NAL, Bengaluru, and low speed wind tunnel at IIT Kanpur were used. Eighteen models (scales 1 : 1 to 1 : 140) were fabricated and more than 4000 blowdowns were carried out. CFD and engineering codes were employed where wind tunnel testing was not feasible. Pressure and load distribution were estimated only through CFD, since earlier validation studies for winged bodies indicated good match with test data for overall force and moment coefficients, especially at design critical Mach numbers. Also, unlike the regular launch vehicle configuration, instrumenting the RLV wing-body model with pressure ports located along the longitudinal and lateral generators is an order of magnitude more complex, due to the thickness and volume availability, especially in the wing, vertical tail and control surfaces.

Figure 7 shows a flowchart of aerodynamic characterization and its end use in launch vehicle system design.

Aerodynamic characterization in ascent phase

Aerodynamic characterization was carried out for liftoff low-speed, high angle of attack conditions, small angle of attack from subsonic to hypersonic flight and stage separation at hypersonic conditions, using a combination of wind tunnel test data, CFD and engineering methods.

The data obtained from low speed tests at high angles of attack and load distribution generated through engineering method (cross-flow theory results matched to test data) were used for structural design, analysis of the base shroud as well as for liftoff simulation studies. Figure 8 shows the sensitivity of normal force coefficient to proximity of launch pad and umbilical tower, and also to wind direction when the vehicle is on the launch pad. This information was also used in choosing liftoff time.

The vehicle configuration in ascent phase was an unconventional combination of winged body mounted on the HS9 booster. Hence, fins were sized for both stability and pitch/yaw/roll control using the movable part of the fins. During this phase, the elevons and rudders were held at null position. Aerodynamic characterization of the

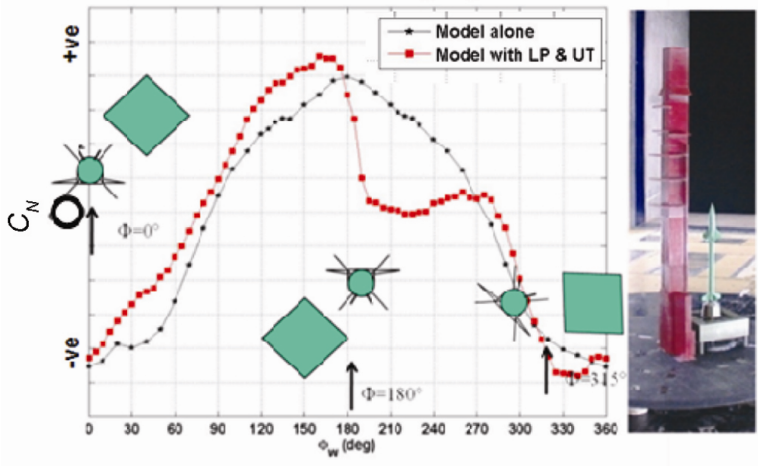

Figure 8. Liftoff aerodynamic characterization showing the sensitivity of normal force coefficients to the launch pad umbilical tower and wind directions.

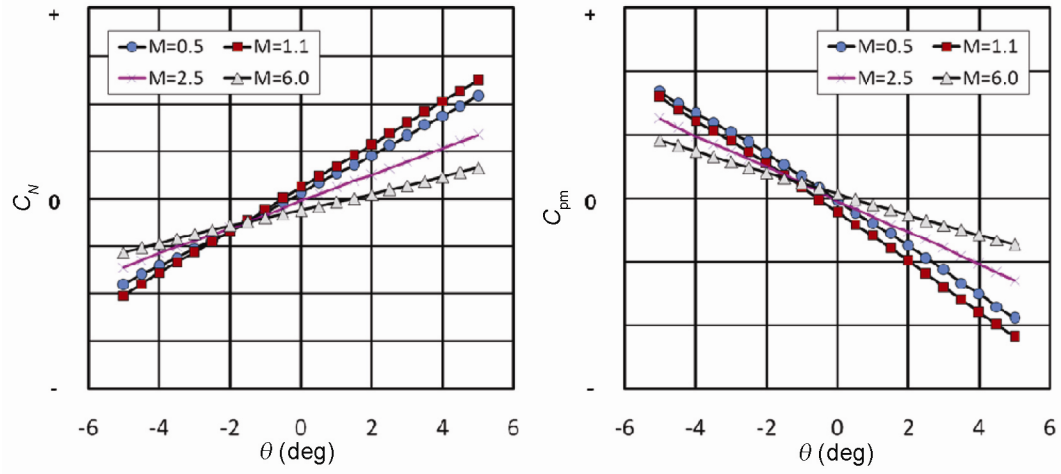

Figure 9. Ascent vehicle normal force and pitching moment coefficients without fin deflection.

vehicle consists of tests with and without fin deflection. Figure 9 illustrates the variation of normal force and pitching moment coefficients for various Mach numbers without fin deflection at various total angles of attack θ with 0° roll angle. This shows the asymmetric nature of the vehicle aerodynamics due to the configuration. The data are crucial input for trajectory and control system design. Peak value for pitching moment coefficient occurred at transonic Mach number and the value decreased with increasing Mach number at supersonic values.

It is not possible to carry out tests for various fin deflections ranging from +30° to –30° for all the fins at various Mach numbers, roll angles and angles of attack. Hence, it was decided to test fins 2 and 4 for obtaining incremental aerodynamic coefficients due to fin deflection, and then suitably transform data to be used for fins 1 and 3. Figure 10 presents incremental normal force coefficient due to fin 4 deflection as estimated using wind tunnel tests and CFD code PARAS-3D at critical Mach number 1.1 for various fin deflections at 0° angle of attack. The slight nonlinearity in the data is visible clearly. It can be observed that CFD prediction and test data match well at this Mach number.

The results for incremental aerodynamic coefficients due to single fin deflection were properly transformed to get aerodynamic coefficients due to various fin deflection combinations which can occur in flight. Few wind tunnel tests carried out at select Mach numbers revealed that the linear superposition adopted led to a difference of ~20% at $M = 1.1$. Fin–fin interference decreased with increase in Mach number. Hence, fin–fin interference was studied in-depth using CFD codes and wind tunnel tests, especially at $M = 1.1$, which was critical from controllability point of view. Combined fin deflection data have been generated through wind tunnel tests to validate the derived fin deflection data from individual fin deflections. In these tests, the fin deflections were limited to 10°, since mission simulation studies revealed that fin deflection in the off-nominal

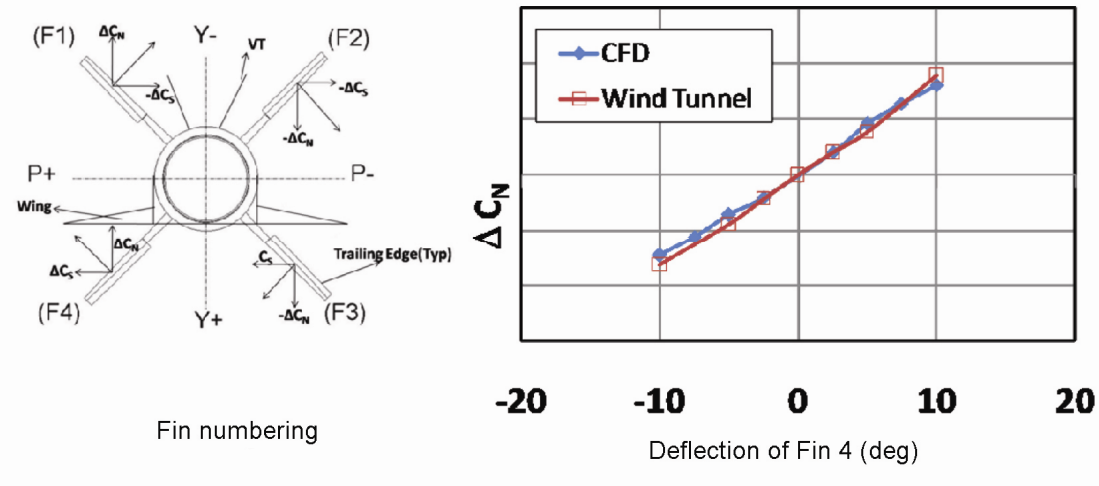

Figure 10. Fin numbering convention and incremental normal force coefficient comparison due to fin 4 deflection.

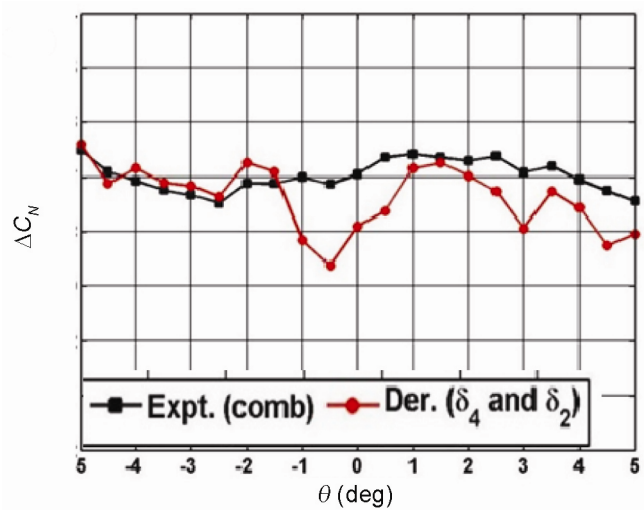

Figure 11. Incremental normal force coefficient due to combination of fin deflections.

case does not exceed 10°. Derived data match with experimental data by about 10% for 13 out of 20 tested cases, for the considered fin deflection range at $M = 1.1$ (Figure 11).

In case of axial force coefficient, base drag coefficient is influenced by the presence of jet. Hence, CFD simulation results were used to correct the wind tunnel test results for base drag coefficient alone, whereas the forebody drag coefficient was obtained from wind tunnel tests.

Hinge moment created due to aerodynamic pressure distribution is an important input for control actuation system design. Hinge moment coefficient acting on the movable fins during ascent phase with change in angle of attack, Mach number and fin deflection were estimated using CFD, since it is difficult to measure hinge moments using conventional balances and measure fin loads alone using a scaled model in wind tunnels.

In order to avoid sudden build-up of undesirable aerodynamic forces, separation of HS9 booster from RLV-TD[3] was planned at an altitude where the dynamic pressure was of the order of 2 kPa. Time march study was carried out to perform separation dynamics analysis and to ensure collision-free separation during the flight. The worst-case time march sequence accounting dispersion band was done till separating distance of $\Delta X = 0.5D$ (D – diameter of HS9 booster), which happened at 1 sec from separation. Aerodynamic coefficients of separating HS9 body were measured for different attitudes, lateral and longitudinal distances from the winged body. The experimental data (Figure 12), indicate that axial force coefficient (C_A) increases gradually up to $\Delta X = 0.3D$ and a sudden jump is observed at $\Delta X = 0.475D$ as HS9 experiences supersonic flow (noticed in Schlieren image in Figure 12). At the starting of the separation ($T = 0$ sec), the HS9 nose is in the wake of RLV and gradually flow momentum increases during its longitudinal movement. Figure 12 also indicates that normal force coefficient (C_N) increases linearly with angle of attack and pitch down moment is generated about the centre of gravity (c.g.) of HS9. The pitching moment coefficient of separating body has negative slope and thus separating HS9 booster is statically stable. It is confirmed that the separating HS9 does not collide with RLV (forebody) even for detrimental trajectory sequence. CFD simulations were also performed to assess the effect of twin retro rocket firing on separation aerodynamics.

The aerodynamics of separated booster was assessed through a combination of wind tunnel tests and CFD simulations. The booster, after separation from the winged body, was statically stable from Mach number 2 to 5 at small angles of attack. At high angles of attack, the booster has a tendency to tumble and the drag coefficient due to tumbling motion was estimated through engineering methods. The aerodynamics of separated winged body at high Mach number and high angles of attack was assessed using CFD. The data were used for

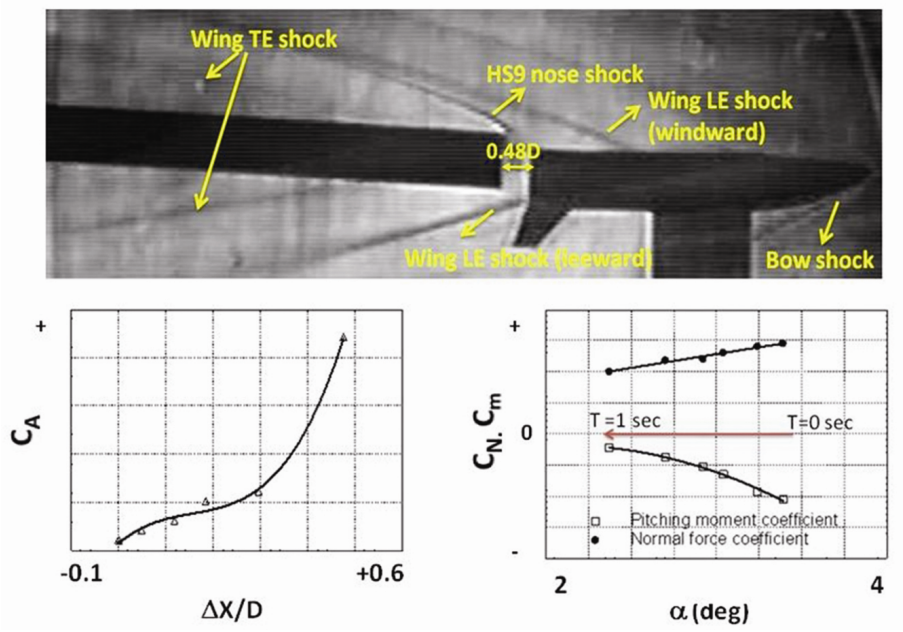

Figure 12. Wind tunnel time march tests for RLV-HS9 separation aerodynamics characterization.

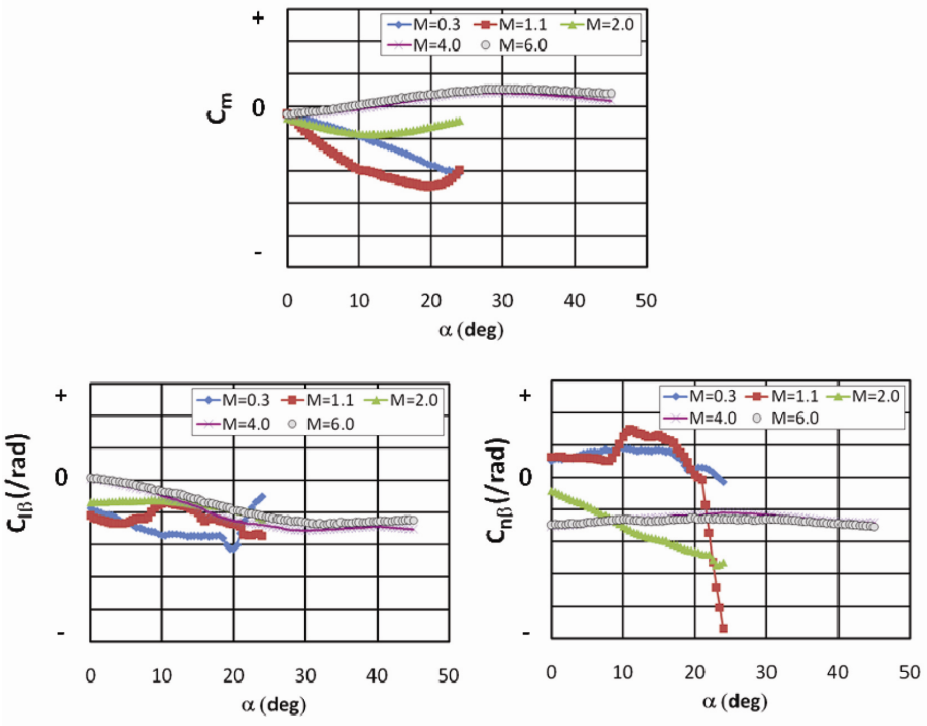

Figure 13. RLV-TD descent phase longitudinal and lateral-directional stability characteristics.

separated body trajectory analysis and range safety studies. Videos obtained during flight also showed that the orientation of the separated booster did not change much, indicating that the vehicle is statically stable.

Aerodynamic characterization in descent phase

The challenge in aerodynamic characterization is the number of variables involved and hence, a huge database spanning Mach number, angle of attack, elevon and rudder deflection was generated.

Figure 13 gives an overview of the stability characteristics in descent phase of RLV-TD. The vehicle longitudinal static stability is indicated by the gradient of pitching moment coefficient (C_m) with angle of attack. The vehicle was statically stable in the operating angles of attack ranging from $M = 2.0$ to low speeds, whereas it was statically unstable at higher Mach numbers. The rolling

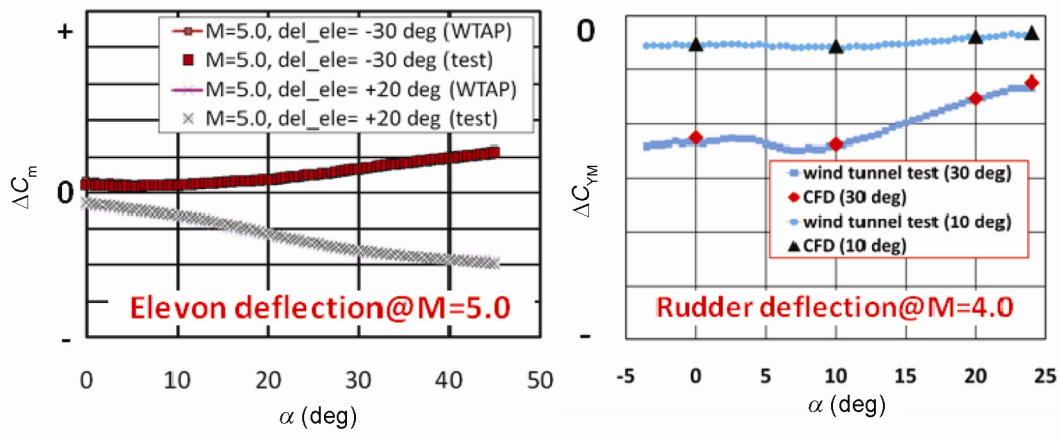

Figure 14. RLV-TD descent phase control surface characterization and comparison of data from wind tunnel tests, CFD and engineering method.

moment coefficient slope with respect to angle of sideslip ($C_{l\beta}$) at various angles of attack was negative, which indicates that the vehicle has dihedral effect at all Mach numbers; this is expected due to the swept double-delta wing and its dihedral angle. The vehicle was directionally stable (positive $C_{n\beta}$) from low speeds up to low supersonic Mach number, above which it was directionally unstable (negative $C_{n\beta}$). This characteristic was similar to the observations for the Space Shuttle, X-34 (refs 4, 5). The control system should be designed to cater to such stability switch-over.

Flight control was through the deflection of elevon from stage separation up to touchdown and rudder was used in the high dynamic pressure phase of descent flight. Control surface deflections produce moments about all three axes due to the distribution of pressure and their placement with respect to centre of gravity/moment reference centre; these moments are used for controlling the attitude of the vehicle. Control surface deflection studies were carried out for both symmetric and asymmetric elevon and rudder deflections to estimate aerodynamic control derivatives such as rolling and yawing moment coefficients due to elevon and rudder deflection. Upward elevon deflection produces pitch-up moment, whereas downward elevon deflection produces pitch-down moment. RLV-TD has negative pitching moment during a major portion of its descent phase and hence, upward elevon deflection is needed to trim the vehicle at the desired attitude. Rudders when deflected symmetrically produce primarily yawing and rolling moments; they produce pitching moment with asymmetric deflection. Rudders were used for pitch trim and hence were deflected inward to correct the negative pitching moment of the basic configuration.

Figure 14 shows the effect of symmetric (same sign for left and right elevon deflection) elevon deflection on incremental pitching moment coefficient at a typical hypersonic Mach number for upward as well as downward deflection of elevon. The agreement between test data and pre-test prediction using engineering code 'WTAP' (utilizing the space shuttle database with suitable corrections for geometry and centre of gravity location) is clearly seen. Elevon effectiveness was better for downward deflection compared to upward deflection. The increase of elevon effectiveness with angle of attack is also more for downward deflection.

Rudders, when deflected, due to their placement in the aft end of the vertical tail, create force and moment coefficients. Figure 14 clearly shows the effect of symmetric rudder deflection (same sign and magnitude for portside and starboard rudder deflection) on incremental yawing moment coefficient at supersonic Mach number. The agreement between test data and CFD code is also clearly seen. Rudder effectiveness reduces at high angles of attack ($\alpha > 10°$) and the rate of reduction is higher for higher rudder deflection. This information was used to tailor the trajectory profile and control surface deflection setting during entry conditions.

Hinge moment coefficient acting on elevon and rudder was obtained by special purpose wind tunnel test (Figure 15). The variation of elevon hinge moment coefficient was found to be linear with elevon deflection up to ±10° and angles of attack up to 10°. It was also observed that the positive deflection of elevon produced higher hinge moment than the negative deflections. Figure 15 shows the variation of elevon and rudder hinge moment coefficients at supersonic Mach number. It can be observed that rudder effectiveness decreases with angle of attack.

Reaction control jets are efficient to control reusable launch vehicles, especially at low dynamic pressure conditions. In this mission, roll RCS jets were fired during low dynamic pressure regime at liftoff. Later, yaw RCS jets were fired at high altitudes after stage separation up to re-entry. The RCS jet effect can be classified as direct jet effect, interference effect and impingement effect[6]. The direct jet effect is due to the momentum of the pure jet.

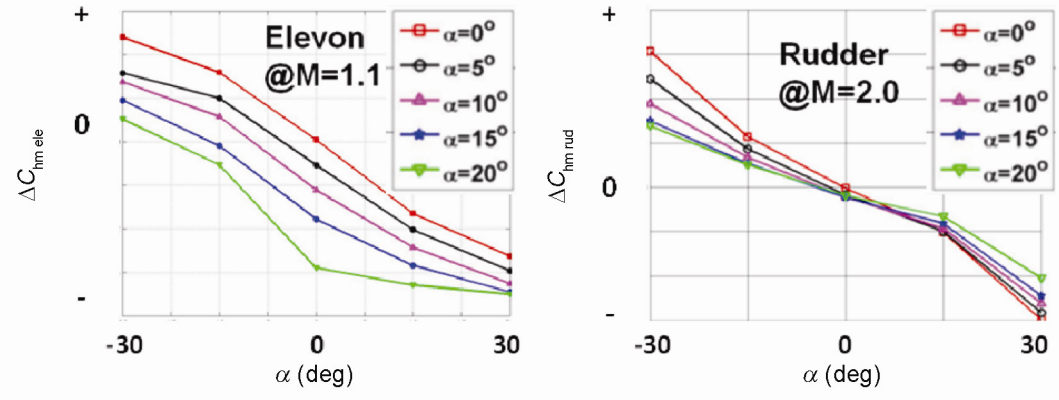

Figure 15. Elevon and rudder hinge moment coefficient characterization through special purpose wind tunnel tests.

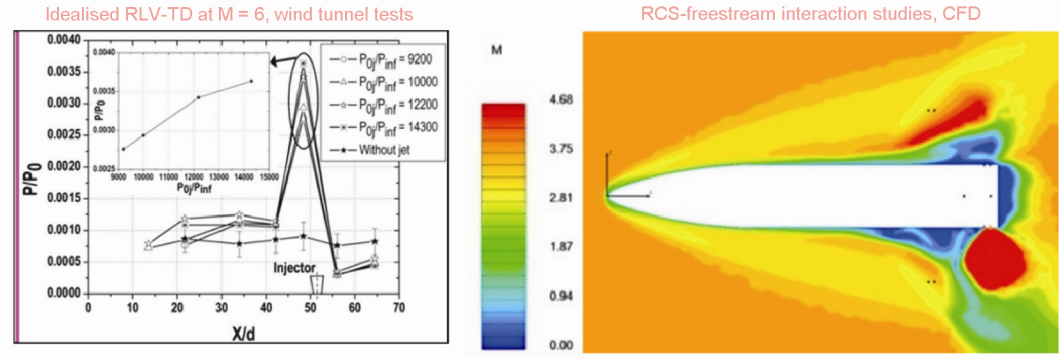

Figure 16. RCS jet-freestream interaction studies through wind tunnel tests and CFD.

The interference effect is due to the change in surface pressure field in the vicinity of the interaction of lateral jet with the freestream flow. The impingement effect is due to the direct impingement of RCS jet on the body surface. RCS jet–freestream interaction resulted in the modification of pressure distribution over the vehicle, and thereby the force and moment coefficients. The RCS jet-freestream interaction studies at hypersonic Mach numbers and high-altitude conditions for an idealized case (Figure 16), indicate complex flow features such as bow shock due to jet injection, separation ahead of the jet, etc.[7]. However, only CFD simulations were used for RCS jet–freestream interaction at high altitudes for the flight scale[8], since wind tunnel testing was not feasible during this timeframe. Interaction for various combinations of thrusters firing (pitch, yaw and roll) at various altitudes (30–75 km) and at various Mach numbers (3–5.3) and, relevant trajectory angles of attack were studied. It was observed that (i) interference generated moments aid the RCS firing, and (ii) there was coupling in roll and pitch when yaw jets were fired due to change in pressure distribution over aft portion of one half of the vehicle. Interference moments increased with dynamic pressure.

Dynamic derivatives are needed for mission studies. For this mission, only some important dynamic derivatives of ascent and decent configurations were estimated based on the literature, relevance to the mission and tools available. For ascent phase, only rotational dynamic derivatives due to pitch/roll/yaw rates have been estimated through an engineering approach using 'CFD-based load distribution'. The method uses the panel-wise distribution of local normal force coefficient at a given angle of attack about which the vehicle acquires the pitch/yaw velocity to obtain the damping derivatives. The load distribution can be obtained from CFD simulations. In this method local slope is assumed constant for small change in instantaneous angle of attack during pitch or yaw motion. The induced local normal force coefficient is obtained by multiplying the ratio of induced local angle of attack to the vehicle angle of attack with the local change in normal force coefficient. The summation of induced local normal force coefficients along the body length is equal to that due to pitch velocity, and the summation of induced local moment about centre of gravity is the moment coefficient due to pitch velocity. The damping derivative due to rate of change of angle of attack is calculated using Sack's relations. The present computation does not include the time lag aspect which is significant at transonic Mach number with high angle of attack, where there is flow separation. However, this effect reduces at higher supersonic and hypersonic Mach numbers.

Dynamic derivatives for the descent phase, pitch and yaw damping have been obtained through wind tunnel 'forced-oscillation' testing for Mach number up to 2. At Mach numbers >2.0, pitch and yaw damping derivatives have been estimated using CFD-based load distribution technique. Roll damping derivative has been estimated using DATCOM methods. The conclusion is that the vehicle has damping in pitch, yaw and roll in the complete descent phase.

Aerodynamic characterization of air data system

Aerodynamic flow parameters such Mach number, angle of attack/sideslip, freestream pressure and dynamic pressure are required for navigation, guidance and control (NGC) system. A flush air data system (FADS) mounted in the nose cap of RLV-TD is proposed for the estimation of air data parameters, using suitable algorithm utilizing flight pressure measurements. The pressure ports conceived in the initial design were 17 and subsequently, this was revised to 9. Pressure measurements were carried out through suitable wind tunnel tests utilizing scale models. The data were used for FADS algorithm calibration. Details of FADS algorithm, its performance in flight and air data parameter reduction are given in detail in a separate paper in this special section. In addition, the complete functional qualification of the FADS system (sensors, conduits, data acquisition system, etc.) was also carried using out a low-speed wind tunnel. Being the maiden flight, FADS was in 'monitoring' mode in this mission.

Aerodynamic uncertainties

The data generated on ground through wind tunnels, empirical correlations and computational resources and their associated uncertainties[9] are crucial for the RLV mission. Once the data are available, the design and implementation of any control system involves the testing for potential errors called uncertainties or dispersions. In the field of experimental aerodynamics measurement, errors may arise due to inbuilt characteristics of measurement instruments, data acquisition systems, testing techniques, etc. Thus, there is a set of errors in wind tunnel measurements, which combines to represent data reproducibility. Further, there are uncertainties in applying the wind tunnel data to flight. These may arise due to Reynolds number scaling, geometric fidelity, aeroelastic distortion differences, real-gas effects, etc. The basis for determining these uncertainties in the descent phase is the difference between flight test measurements and pre-flight predictions found for similar (in configuration or mission) vehicles like space shuttle and light combat aircraft (LCA). For the ascent phase, source of data is the difference between pre-flight and flight data of ISRO launch vehicles.

The ascent configuration, though an unconventional one, can be compared to other launch vehicles because of low angle of attack flight profile. Repeat tests were done for assessing the repeatability error. An engineering judgment for tunnel-to-tunnel variations was arrived at after studying other launch vehicle wind tunnel variations, with testing in different facilities. Tunnel-to-flight differences were taken to be 50% higher than tolerance (both repeatability error and tunnel-to-tunnel variations) based on space shuttle literature[10]. This information was used to arrive at expected differences for tunnel–flight consideration. The uncertainties were generated for maximum expected angle of attack in flight and different components were added in root sum square manner.

For descent configuration, it was observed that uncertainty obtained from repeat tests was much smaller than that obtained from data comparison for multiple tunnels and models. The Space Shuttle had an extensive wind tunnel testing programme involving testing with different models, using different tunnels and different testing techniques. The basis for determining tunnel-to-flight uncertainties was to observe differences between the historical flight test measurements and the pre-flight predictions found for many similar vehicles. Since RLV-TD and Space Shuttle have geometric, mission and aerodynamic data similarity, uncertainty data for tunnel to flight can be used from the space shuttle literature with additional 20% to account for limited wind tunnel test data. The uncertainties were used in a correlated manner and perturbation of simultaneous parameters implemented considering reduction of probability for simultaneous occurrence of multiple cases. Figure 17 shows the various components of dispersion on aerodynamic data.

Pre-flight acoustic envelope

Aeroacoustic levels are generated due to the unsteady pressure fluctuations of flow over the aerospace vehicle at high Reynolds number and during liftoff due to the propulsive jet. Peak pressure fluctuations occur in the transonic flow conditions due to shock oscillation, shock-induced flow separation and reattachment apart from fluctuations in the boundary layer. High acoustic levels can cause higher vibration excitation on the structural components, avionics packages, propulsion elements like the valves, igniters, plumbing, etc. Low-level excitation for a long period may cause structural failure due to fatigue. Therefore, the aeroacoustic characterization and evolving pre-flight envelope are important aspects for flight-worthiness of an aerospace vehicle.

Compared to launch vehicle acoustics, the wing-body configuration results in high acoustic levels due to vortex-dominated flow, transonic shock–vortex interaction, vortex burst and the upstream influence of control surface deflections on the above flow phenomena. The adequacy

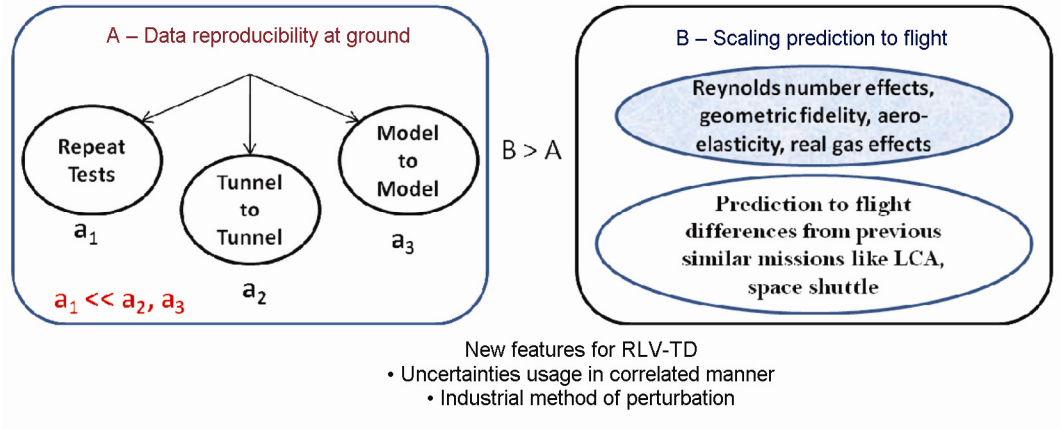

Figure 17. Various components of aerodynamic dispersion accounted in the RLV-TD database.

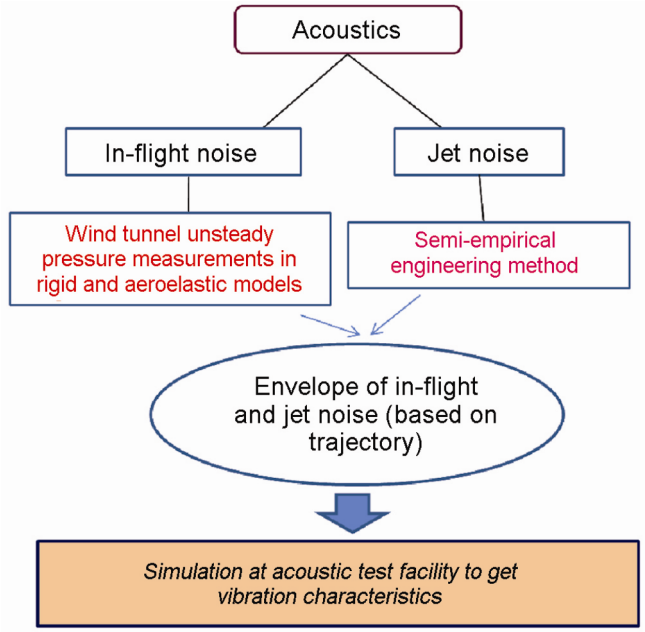

Figure 18. Sources of acoustics and prediction methodology for acoustic test simulations.

of subscale wind tunnel tests for arriving at the vibro-acoustic design environments has been demonstrated for the Space Shuttle ascent flight, where good correlations were observed with the wind tunnel acoustic data[11]. Acoustic levels during liftoff due to the HS9 solid booster jet was predicted using spectrum source distribution (SSD) technique. An envelope of the jet noise for various liftoff heights up to vehicle clearing umbilical tower was obtained. A dispersion of +5 dB was added to the jet acoustic prediction. The complete in-flight noise levels were estimated using the unsteady pressure measurements on a scaled model. The core base shroud level was obtained from the aeroelastic test using a 1:15 scale aeroelastic model. Inter-stage pre-flight measurement was not available; therefore, the acoustic level at the inter-stage was estimated using unsteady pressure ports on the aft fuselage. Power spectral density (PSD) data were scaled to flight conditions using dynamic pressure and boundary layer parameter. Displacement thickness and geometric parameters were used as scaling parameters for the attached and separated flow conditions respectively. The wind tunnel PSD data were scaled to flight up to 800 Hz and is further linearly extrapolated up to 8000 Hz in octave band to meet the flight conditions. The one-third octave band was generated for each ports and enveloped across angles of attack, control surface deflections (elevon and rudder) for each Mach number corresponding to the upper bound trajectory to get the environmental test levels (ETL). The ETL levels were simulated in the acoustic facility to obtain the vibration characteristics. The vibration details were further used for flight acceptance tests for stages, actuator systems and avionics packages. Figure 18 provides an overview of the methodology used for acoustics.

Aerodynamic performance in flight

Figure 19 shows the post-flight estimated normal and axial force coefficients in ascent phase. Normal acceleration measured in ascent phase, though the angle of attack is small, is considerably higher than the values obtained in regular launch vehicle flights because of the winged-body configuration and fins which create reasonable normal acceleration levels. Hence, normal force coefficient has been estimated for the ascent phase (Figure 19) along with pre-flight values. The normal force coefficient was found to match well within the pre-flight dispersion bands at all Mach numbers. Side force coefficient could not be estimated because the acceleration levels in the perpendicular direction were very low. Post-flight estimated axial force coefficient was within pre-flight dispersion, except at transonic Mach numbers where flight indicated a slightly higher value. This was addressed in

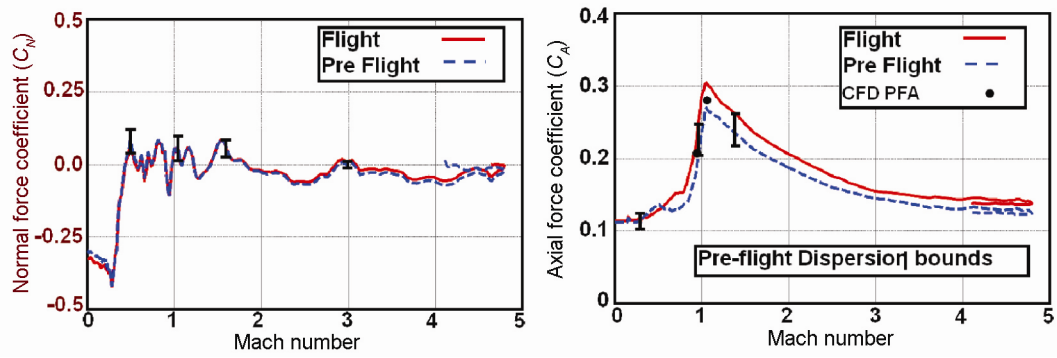

Figure 19. Pre-flight predictions and post-flight estimates of C_N and C_A in the ascent phase.

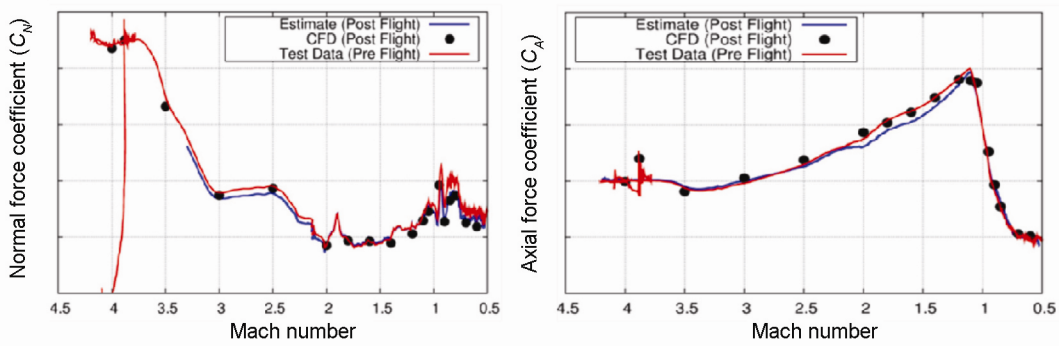

Figure 20. Pre-flight predictions and post-flight estimates of C_N and C_A in the descent phase.

the post-flight CFD simulations, and the results indicated that minor geometric changes which were not simulated in wind tunnel test model caused this minor deviation in axial force coefficient.

Extended Kalman Filter (EKF)-based estimation methodology was utilized to estimate aerodynamic coefficients for the decent phase. The advantages are: (1) all the flight parameters are matched and (2) it is possible to obtain the estimation error bounds.

The normal and axial force coefficients during descent phase were estimated (Figure 20). Post-flight estimate for normal force coefficient matched well with test data from high supersonic Mach numbers till $M = 1$. Below $M = 1$, the estimate was lower than expected, but within the pre-flight dispersion bands. CFD data were closer to the estimate than test data. Post-flight estimate for axial force coefficient matched well with test data at all Mach numbers. CFD prediction for pressure drag coefficient was added to skin friction drag estimate from engineering methods, and the total axial force coefficient matched well with test data and post flight estimate.

Hinge moment acting over elevon and rudder was estimated from in-flight actuator chamber pressure measurements. Wind tunnel data were observed to be in line with the flight estimate for elevon hinge moment, except at low transonic Mach numbers (Figure 21). CFD-based post-flight prediction for elevon hinge moment agreed well with flight data for $M > 1.2$. Wind tunnel data as well as CFD results agreed well with flight estimate for rudder hinge moment.

In flight, it was also observed that roll rates were induced due to yaw RCS jet firing as predicted by CFD before flight, but the magnitude observed in flight was found to be higher than the predicted value. Pitch rates (coupling) were also observed, but the magnitude was higher and increased with dynamic pressure. CFD simulations were carried out for post-flight analysis, which indicated the sensitivity of the interference effect for a given Mach number, to the flight jet-to-freestream pressure ratio.

For dynamic derivatives, only roll damping was estimated since significant roll rates were excited in flight especially at transonic Mach numbers, which may be due to low inertia in the roll axis. The initial flight estimate (Figure 22) indicates a higher damping than prediction using DATCOM methods at Mach numbers less than 2 up to high subsonic Mach numbers, this is being investigated by another engineering approach based on steady-state CFD results.

Fifty-three pressure ports over fuselage, wing, vertical tail, rudder and fuselage base were instrumented in flight and aerodynamic external pressure measurements were obtained both in ascent and descent phases of flight. The comparison of data indicates that (1) prediction is better in ascent phase compared to descent phase and (2) in

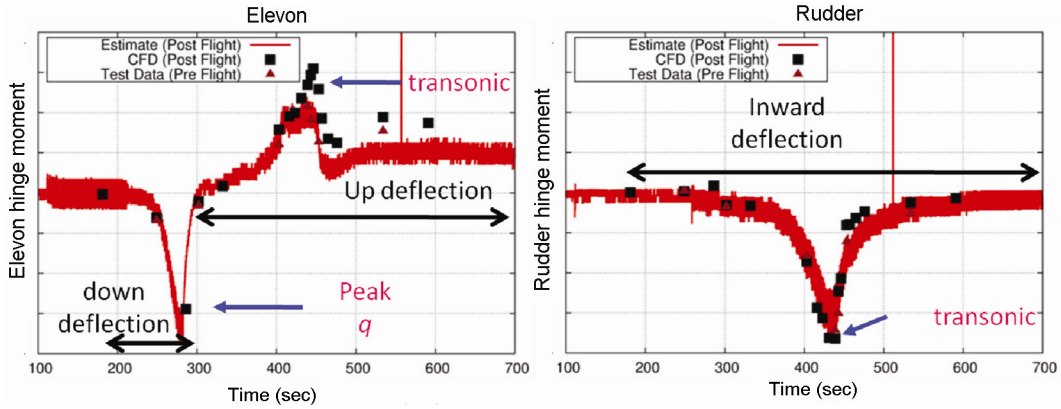

Figure 21. Elevon and rudder hinge moment comparison.

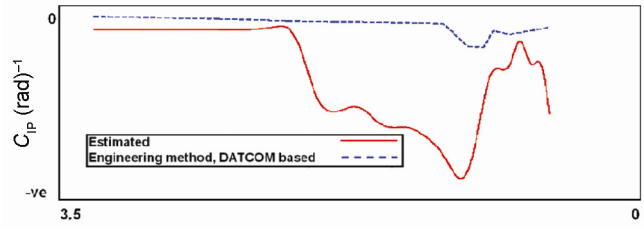

Figure 22. Roll damping derivative in descent phase indicating more damping in flight than predicted.

descent phase, the prediction is closer to flight at $M > 1$ compared to lower Mach numbers. Figure 23 provides a view of the ports used for flight measurements. Comparison for coefficient of pressure (C_p) data estimated through flight pressure measurements and CFD simulation results over two wing sections during descent phase is shown in the figure for a typical supersonic Mach number and high angle of attack combination. Since, preflight pressure and load computation were only through CFD, the flight data provide confidence in the usage of data at design Mach numbers for a typical re-entry vehicle (all critical load cases are at $M > 1$).

Pressure was acquired though flight measurements in all the nine FADS ports, during ascent and descent phases. Air data parameters were derived using FADS algorithm in post-flight analysis phase and the following features were observed: (1) angle of attack/sideslip could be estimated within 1 deg accuracy; (2) the accuracy of Mach number derived through FADS was better at $M < 1$. Post-flight analysis also revealed that calibration parameter, which is a function of port location and flow parameters (M, α, β), is sensitive to C_p dispersion, especially in supersonic Mach numbers.

Flight-measured acoustic levels were obtained from all the six microphones (five external and one internal) from liftoff to splashdown. The measured data were processed on-board to get the sound pressure levels (SPL) at discrete time (250 ms) and transmitted back to the base stations. At liftoff, the flight overall sound pressure level (OASPL) of the core base shroud peaks at 155.5 dB due to its proximity to the booster jet. The measured liftoff noise is higher by 2.8 dB compared to the predicted upper bound. In the ascent flight, the OASPL comparison with estimates is good in the transonic regime. However, in the supersonic regime, the estimates are under-predicted. The maximum difference of predicted value to flight data is around 6 dB in the descent phase. Figure 24 provides a summary of OASPL prediction and flight data.

In addition, in this flight, the effect of RCS jet firing was felt in the acoustic measurements at liftoff low dynamic conditions.

Observations and lessons learnt regarding aerodynamic design, characterization and flight parameter estimation

(1) Engineering methods, CFD tools, computing resources and wind tunnel facilities in-house and in the country, worked in a harmonious manner for configuration design studies and the final aerodynamic characterization of this vehicle, under ascent and descent phases. A recently commissioned 1 m hypersonic tunnel has been utilized for generation of aerodynamic data at hypersonic Mach number. The success of the mission also underlines the maturity of CFD tools.

(2) One of the important lessons learnt in the configuration evolution phase of ascent vehicle is that keeping a winged-body configuration on top of a cylindrical configuration with fins poses severe aerodynamic and control issues. The validity of the choice of configuration with double-delta wing and twin canted vertical tails has been successfully demonstrated in the descent phase of the flight.

(3) The effort involved in the aerodynamic characterization of aerodynamically controlled vehicle spanning a huge parameter space, is orders of magnitude higher, compared to a conventional expendable launch vehicle. For this scaled demonstrator, thousands of data tables have been generated as against few tens of data tables for regular launch vehicles.

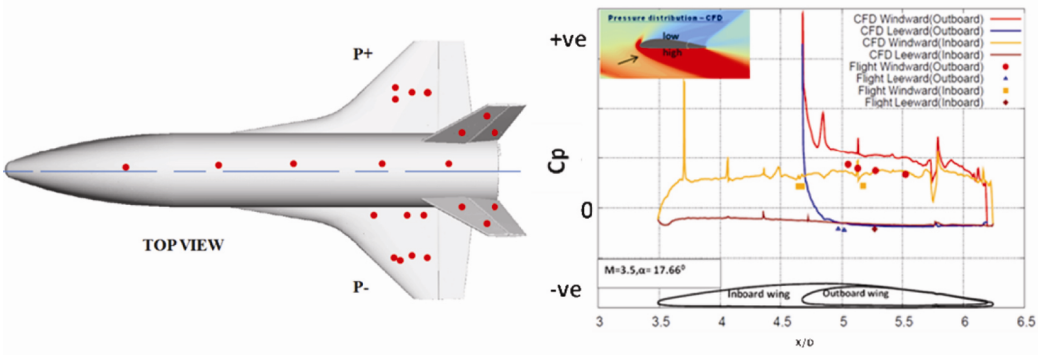

Figure 23. Distribution of static pressure ports on the leeward side of RLV-TD and C_p comparison between flight data and CFD results over wing sections in descent phase.

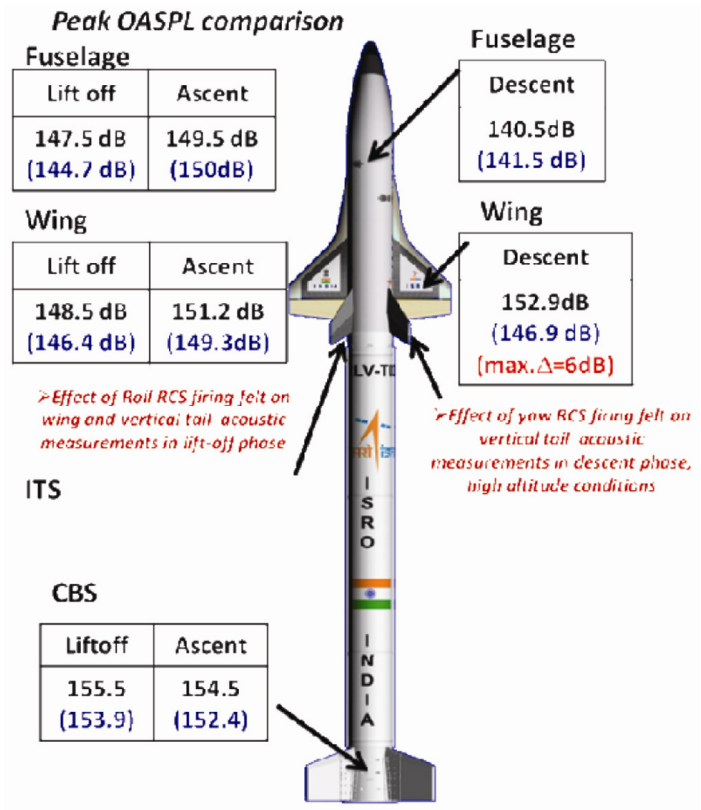

Figure 24. Acoustic levels over RLV-TD in ascent and descent phases (flight-measured values – blue, pre-flight predicted – black).

(4) As observed in this mission, liftoff aerodynamics is significant as the vehicle had to clear the launch tower which was three times longer. Several wind tunnel tests had to be carried out to cater to varying wind direction and at various positions of the vehicle relative to the tower. Also, the time of launch became critical for this mission due to liftoff-related aerodynamics. The magnitude of the problem may be reduced if the launch tower is tailor-made for the mission.

(5) Only few important dynamic derivatives were used in this mission due to planar trajectory. Many cross-derivatives may have to be estimated precisely for similar future missions, for which new facilities such as spin tunnel and very large low speed tunnels are required.

(6) Fins were used as control devices in ascent phase. Only two control surfaces, elevon and rudder were used in this configuration in descent phase, unlike the other winged reusable launch vehicles where a body flap was also used. The behaviour related to the control surface deflection (sign and magnitude) predicted before flight was observed in flight too, in both ascent and descent phases.

In this flight, rudder was used for pitch trim also, in the descent phase.

(7) The complex interference studies, such as fin-to-fin interference effect, and RCS jet effect on aerodynamics could be captured well by CFD tools. Wherever possible, all the above have been validated through tests. However, it is prudent to employ extensive scale-model testing using wind tunnels for detailed RCS–freestream interference characterization. This in turn, necessities the augmentation of the existing testing facilities.

(8) The dispersion bands have been arrived at based on wind tunnel tests within the country and information from aircraft industry, the literature based on Space Shuttle Orbiter, X-34, etc. However, it is better to carry out aerodynamic characterization using various scale models for a full-scale flight in future.

(9) Parameter estimation methodology has been successfully applied in both ascent and descent phases of flight involving a large number of variables and high angles of attack. Normal force coefficient, pitching moment coefficient as well as roll damping derivatives have been estimated for the first time.

(10) A good match with flight data was observed in both ascent and descent phases of flight. Axial force coefficient experienced in ascent flight was slightly higher than the pre-flight nominal data, but a thorough post-flight analysis brought in the effect of minor geometrical differences. In the descent phase, axial force coefficient was well within the maximum dispersion band value of 0.02. Normal force coefficient in the descent phase matched with pre-flight data within 0.06.

(11) Pressure measurements over the winged body in various flight regimes indicated the goodness of CFD-based prediction methodology at critical Mach numbers ($M > 1$) and flight angles of attack. However, it is necessary to carry out wind-tunnel tests for pressure measurement, if possible. Flight experience with FADS indicated that dispersion bands have to be adhered to, especially at $M > 1$. Tight control on port locations and pressure measurement accuracy are needed for prediction using FADS algorithm, especially for Mach number prediction.

(12) The measured acoustic levels are within the pre-flight envelope. The peak acoustic level match is good and spectrum is comparable to the pre-flight spectrum for most of the components. Acoustics due to the roll RCS jet firing is seen as small jumps in the OASPL levels during liftoff at low dynamic pressure condition.

Conclusion

The maiden successful flight of ISRO's RLV-TD took place in May 2016. The complete aerodynamic design, analysis and database generation for this aerodynamically intensive vehicle has been carried out through ground-based facilities such as wind tunnels, CFD simulations and engineering methods. Parameter estimation techniques have been applied in both ascent and descent phases of flight, and aerodynamic parameters have been reconstructed using flight data. Overall, the present flight data comparison gives high level of confidence in using the ground-based data generation techniques for a wing-body configuration.

1. Ashok, V. and Babu, T. C., Parallelization of Navier–Stokes code on a cluster of workstations. In Proceedings of the 6th International High Performance Computing Conference, HiPCC'99, Springer, Berlin, 1999, pp. 349–353.
2. Manokaran, K., Vidya, G. and Goyal, V. K., A simple procedure for computation of aerodynamic coefficients with control surface deflection for a winged RLV. In Proceedings of a Symposium on Applied Aerodynamics and Design of Aerospace Vehicle (SAROD) 2005. Recent Trends in Aerospace Design and Optimization, Hyderabad, 8–9 December 2005, pp. 191–202.
3. Yuvaraj, R. *et al*., Challenges in solid booster separation dynamics analysis for a winged body. *J. Aerosp. Sci. Technol.*, 2017, **69**(3A), 502–514.
4. Surber, T. E. and Olsen, D. C., Space shuttle orbiter aerodynamic development. *J. Spacecraft*, 1978, **15**(1), 40–47.
5. Brauckmann, G. J., X-34 vehicle aerodynamic characteristics. *J. Spacecr. Robot.*, 1999, **36**(2), 229–239.
6. Iliff, K. W. and Shafer, M. F., Space Shuttle Hypersonic Aerodynamic and Aerothermodynamic Flight Research and the Comparison to Ground Test Results, NASA-TM 4499, June 1993.
7. Desikan, S. L. N., Saravanan, R., Subramanian, S., Sivaramakrishnan, A. E. and Pandian, S., Investigation of supersonic jet interaction with hypersonic cross flow. *ASME J. Fluid Eng.*, 2015, 137/101101-1, doi:10.1115/1.4030393.
8. Vidya, G., Manokaran, K. and Jeyajothiraj, P., Aerodynamic interference effect on a winged body due to supersonic lateral jet in cross flow. In Symposium on Applied Aerodynamics and Design of Aerospace Vehicle (SAROD 2015), Thiruvananthapuram, 3–5 December 2015.
9. Vidya, G. *et al.*, Aerodynamic design, characterization and parameter estimation of RLV-TD from flight data. *J. Aerosp. Sci. Technol.*, 2017, **69**(3A), 423–439.
10. Young, J. C. and Underwood, J. M., Development of aerodynamic uncertainties for the space shuttle orbiter. *J. Spacecraft*, 1983, **20**(6), 513–517.
11. Dougherty, N. S. and Guest, S. H., A correlation of scale model and flight aeroacoustic data for the space shuttle vehicle, AIAA-84-2351, AIAA/NASA 9th Aeroacoustics Conference, Williamsburg, Virginia, 15–17 October 1984.

ACKNOWLEDGEMENTS. We acknowledge the work carried out by the team headed by Shri V. Nagarajan and Dr G. K. Suryanarayana (NTAF, NAL, Bengaluru) and also the team headed by Prof. Kamal Poddar and Prof. Sanjay Mittal (NWTF, IIT Kanpur). We also thank the reviewers for their valuable suggestions.

doi: 10.18520/cs/v114/i01/48-63